Welcome to XAFS: a friendly but not so short tutorial

3. EXAFS theory

P. Fornasini

Department of Physics, University of Trento, Italy - December 2014

Contents

In the Second Part of this Tutorial, we have seen that, within a set of reasonable approximation (golden rule, one-electron, electric dipole, sudden), the absorption cross section in the EXAFS energy region can be expressed as

$$\sigma_{\rm el}(\omega) \;=\; \frac{\pi e^2 \omega}{\epsilon_0 c}\; |\,\langle\,\psi_f|\;\hat\eta\cdot\vec r\,|\psi_i\,\rangle\,|^2\;\; S_0^2\;\rho(\epsilon_f)\,. \tag{1}$$

In the EXAFS region, the density of final states $\rho(\epsilon_f)$ varies slowly and monotonously. EXAFS oscillations are thus described by the matrix element $|\langle\psi_f|\hat\eta\cdot\vec r|\psi_i\rangle|^2$. The structural information is contained in the one-electron final state $|\,\psi_f\rangle$.
In the following, we want to find the relation between local structure and EXAFS oscillations. For concreteness, we consider the contribution of a K edge to the absorption coefficient.
We start by supposing that $S_0^2 = 1$, say that intrinsic inelastic transitions are negligible; their contribution will be taken into account later on.

1 The atomic absorption coefficient

For an isolated atom, the final state $|\,\psi_f^0\rangle$ is represented by a photoelectron which moves away from the atom as an outgoing wave, and the absorption coefficient is

$$\mu_0 \;=\; n\,\sigma_0 \;\propto\; \left|\,\langle\,\psi_f^0|\;\hat\eta\cdot\vec r\,|\psi_i\,\rangle\,\right|^2\,, \tag{2}$$

where n is the atomic number density (number of atoms per unit volume) and σ_0 is the absorption cross section.
In the energy region between two consecutive absorption edges, the atomic absorption coefficient decreases monotonically as a function of the photon energy $\hbar\omega$ (Fig. 1); this trend is generally expressed as a function of the photon wavelength λ by the Victoreen empirical law

$$\mu_0/\rho \;=\; C\,\lambda^3 \;-\; D\,\lambda^4\,, \tag{3}$$

where C and D are two constants.
Values of the mass attenuation coefficients μ_0/ρ for elements and selected compounds are available at the web site of NIST [1]. Efforts to improve the experimental accuracy of mass attenuation coefficients are made by several researchers [2, 3, 4]. A tutorial calculation of the attenuation coefficient of hydrogen can be found in Section 7.1 of [5].

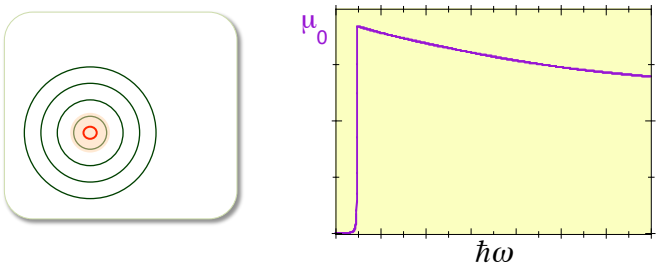

Fig. 1: The outgoing photo-electron (left) and the atomic absorption coefficient of an isolated atom (right).

The photo-electron wave-number

The dynamical properties of the photo-electron are characterised by the wavelength λ or by the wave-number $k = 2\pi/\lambda$ (don't confuse with the analogous quantities of X-ray photons). The photoelectron wave-number k is connected to the photo-electron energy ϵ_f and to the photon energy $\hbar\omega$ by

$$k \;=\; \sqrt{(2m/\hbar^2)\;\epsilon_f} \;=\; \sqrt{(2m/\hbar^2)\;(\hbar\omega - E_b)} \tag{4}$$

where E_b is the core electron binding energy.
Numerically, if k is measured in Å^{-1} and ϵ in eV,

$$k \;=\; 0.51233\,\sqrt{\epsilon}\,.$$

The energy $\epsilon_f = \hbar\omega - E_b$ and the corresponding wave-number k refer to a photo-electron that is completely free, say at a relatively large distance from the initial core orbital.
Photo-electron wave-number k (left) and wavelength λ (right) are shown in Fig. 2 as a function of the photo-electron energy ϵ_f. Note the little variation of λ for energies ϵ_f larger than 200-300 eV.

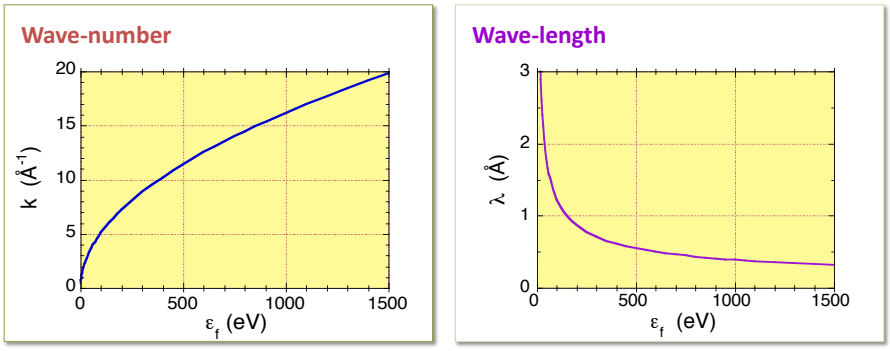

Fig. 2: Photo-electron wave-number k (left) and wavelength λ (right) as a function of the photo-electron energy $\epsilon_f = \hbar\omega - E_b$.

2 Non-isolated atom: the EXAFS function

If the absorber atom is non-isolated (molecular gases, condensed systems) the photo-electron can interact with the surrounding atoms and undergo scattering (Fig. 3, right). In the EXAFS region, the photo-electron energy is much larger than the electron–atom interaction energy, so that the interaction causes a weak perturbation to the the final state:

$$|\psi_f\rangle = |\psi_f^0 + \delta\psi_f\rangle. \tag{5}$$

and the absorption coefficient becomes

$$\mu(\omega) \propto \left|\langle \psi_f^0 + \delta\psi_f | \hat{\eta}\cdot\vec{r}\,|\psi_i\rangle\right|^2. \tag{6}$$

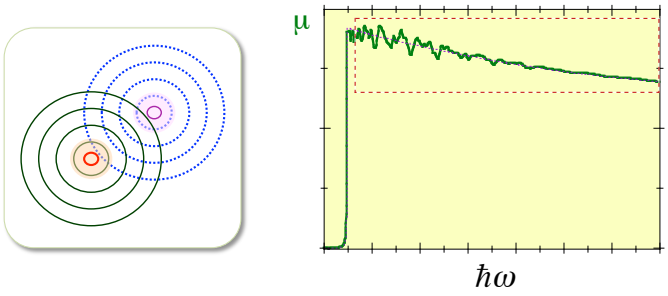

Fig. 3: The outgoing and back-scattered photo-electron (left) and the absorption coefficient of a non-isolated atom (right).

The perturbation $\delta\psi_f$ corresponds phenomenologically to an incoming wave, whose presence modifies the superposition integral of the final state with the initial core state ψ_i in the matrix element with respect to (2).
The EXAFS function is defined as the difference between the actual absorption coefficient μ and the atomic absorption coefficient μ_0, normalized to μ_0 (Fig. 4):

$$\chi(k) = \frac{\mu - \mu_0}{\mu_0} \tag{7}$$

and is generally expressed as a function of the wave-number k (4) rather than of the energy. The amplitude of the EXAFS oscillations ranges typically between 1 and 10 % of the absorption coefficient.

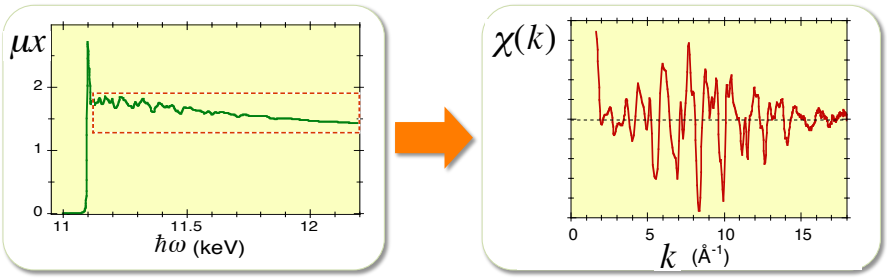

Fig. 4: Left: experimental absorption coefficient μx as a function of photon energy. Right: corresponding normalised EXAFS function (7).

Note: What one actually measures is the product μx, where x is the sample thickness, and the corresponding product $\mu_0 x$. The (generally unknown) sample thickness x is anyway cancelled in (7).

We can now insert the absorption coefficients (2) and (6) in the EXAFS function (7) and express the matrix elements as superposition integrals of wave-functions. By neglecting the term of second order in $\delta\psi_f$ (which anyway would not produce oscillations), the EXAFS function can be expressed as

$$\chi(k) \;=\; \frac{2\mathrm{Re}\int d\vec{r}\;\left[\psi_f^{0*}(\vec{r})\;\hat{\eta}\cdot\vec{r}\;\psi_i(\vec{r})\right]\;\left[\delta\psi_f^{*}(\vec{r})\;\hat{\eta}\cdot\vec{r}\;\psi_i(\vec{r})\right]}{\int d\vec{r}\;\left|\psi_f^{0*}(\vec{r})\;\hat{\eta}\cdot\vec{r}\;\psi_i(\vec{r})\right|^2} \tag{8}$$

The second factor in the integral at the numerator of (8) is responsible for the interference between the outgoing and the incoming wave-functions. The leading contribution to the integral is given by the limited spatial region of the core orbital, which thus represents both the *source* and the *detector* for the photo-electron that probes the surrounding structure.

3 Approximate derivation of EXAFS

A number of different but equivalent derivations of the EXAFS function (8) have been proposed [6, 7, 8, 9]. None of them is however sufficiently simple for an introductory account.
In the following, we will highlight the basic concepts from a phenomenological point of view. Only ideal systems composed of atoms frozen at their equilibrium positions are at first considered; thermal disorder is introduced later on.

3.1 Two-atomic system

The simpler system consists of two atoms, an absorber A and a back-scatterer B; let R be the distance between the two nuclei (Fig. 5). For a given value $\hbar\omega$ of the energy of the absorbed photon, the quantum state of the emitted photoelectron is characterised by the wavenumber k, defined in (4). The photo-electron is subjected to the potentials of the emitting atom A and of the scattering atom B, which are generally approximated by dividing the space into three regions (Fig. 5), corresponding respectively to:

I - a spherically symmetric attractive potential centred on atom A;
II - a constant *inner potential*, connected to the potentials of regions I and III;
III - a spherically symmetric attractive potential centred on atom B.

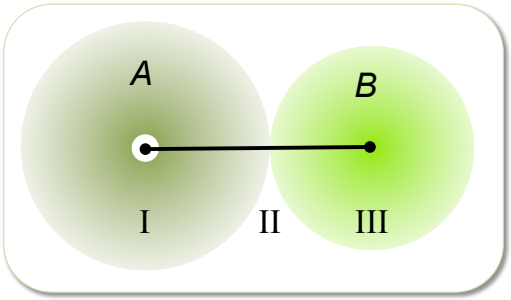

Fig. 5: Absorber atom A and back-scatterer atom B at a distance R. The coloured regions I and II schematically represent the spherically symmetric potentials created by the two atoms, the remaining region II represents the inner potential (muffin-tin approximation). The small white circle at the centre of region I schematically represents the $1s$ core orbital.

The wavefunction ψ_i of the initial $1s$ core state of angular momentum $\ell = 0$ is confined within the core volume schematically represented by the white circle at the centre of region I in Fig. 5. Also the final state wavefunction ψ_f^0 for the isolated atom, of angular momentum $\ell = 1$, has to be known only within the core volume at the centre of region I, in order to evaluate the superposition integrals of Eq. (8).

Actually, the explicit knowledge of ψ_i and ψ_f^0 is not necessary to calculate the EXAFS function (8). It is sufficient to understand how the perturbation $\delta\psi_f$ develops along the photo-electron path $A \rightarrow B \rightarrow A$ and to evaluate its superposition integral with the initial core state ψ_i.

The photo-electron emission is more probable in the direction of polarisation of the photon beam; the angular part of the outgoing wavefunction depends on the dipole term $\hat{\eta} \cdot \vec{r}$. Let us focus our attention on the radial part of the wavefunction.

At the centre of region I, corresponding to the core orbital, the outgoing photo-electron wavefunction is $\psi_f(0) = \psi_f^0(0)$, the same as for an isolated atom. At the border of region I, the radial part of the photo-electron wavefunction can be approximated, for high enough energies ($kr \gg 1$), as

$$\psi_f^0(0)\ \frac{e^{ikr}}{2kr}\ e^{i\delta_1}\,, \tag{9}$$

where k is the wavenumber defined in (4) and the phase-shift δ_1 takes into account the effect of the potential of region I.

Let us now consider the interaction between the photo-electron and the atom B in region III. If the photo-electron has high enough energy, the interaction is important only with the nucleus and the inner electrons of atom B. We can then restrict the scattering to a spatial region very small with respect to the interatomic distance R (*small atom approximation*) and neglect the curvature of the wave impinging on atom B (*plane wave approximation*).
Within these approximations, the scattering process is described in terms of a complex amplitude of back-scattering from atom B in the direction of atom A, $f(k,\pi)$, which can be expressed as a function of the partial-wave phase-shifts δ_ℓ [10] as

$$f(k,\pi)\ =\ (1/k)\ \sum\nolimits_{\ell=0}^{\infty}\ (-1)^\ell\,(2\ell+1)\,e^{i\delta_\ell}\ \sin\delta_\ell \tag{10}$$

At the border of region III, the radial part of the backscattered wave is approximated as

$$\underbrace{\left[\psi_f^0(0)\ \frac{e^{ikR}}{2kR}\ e^{i\delta_1}\right]}_{\text{wave impinging on B}}\quad f(k,\pi)\quad \underbrace{\left[\frac{e^{ikr'}}{r'}\right]}_{\text{scattered by B}} \tag{11}$$

where r' is the distance from atom B.

At the absorber core site (centre of region I), the final wave function is obtained by substituting $r' = R$ in (11) and adding a further phase-shift δ_1 to account for the potential of region I.

The final wavefunction at the core site can be conveniently expressed as

$$\psi_f^0(0)\ \ \frac{1}{2k}\ \underbrace{e^{i\delta_1}}_{\text{inter.}}\ \underbrace{\frac{e^{2ikR}}{R}}_{\text{propag.}}\ \underbrace{f_B(k,\pi)}_{\text{inter.}}\ \underbrace{\frac{e^{2ikR}}{R}}_{\text{propag.}}\ \underbrace{e^{i\delta_1}}_{\text{inter.}}, \tag{12}$$

say as the product of two types of factors: *a)* factors describing the interaction of the photoelectron with atoms A and B, *b)* factors describing the propagation of the photoelectron from atom A to atom B and and from atom B to atom A. Such a basic structure is shared by more sophisticated approaches, which can take into account also multiple scattering (MS) events.

If the result expressed by eq. (12) is properly inserted into eq. (8), one gets

$$\chi(k)\ =\ 3(\hat{\boldsymbol{\eta}} \cdot \hat{\mathbf{R}})^2\ \frac{1}{kR^2}\ \mathrm{Im}\left\{f_B(k,\pi)\ e^{2i\delta_1}\ e^{2ikR}\right\}. \tag{13}$$

By separating modulus and phase of the complex backscattering amplitude and grouping the phase terms,

$$f_B(k,\pi)\ e^{2i\delta_1}\ =\ |f_B(k,\pi)|\ e^{i\phi(k)}, \tag{14}$$

we can write Eq. (13) in real form:

$$\chi(k) \;=\; 3(\hat{\boldsymbol{\eta}}\cdot\hat{\mathbf{R}})^2\,\frac{1}{kR^2}\;|f_B(k,\pi)|\;\sin\left[2kR+\phi(k)\right]. \tag{15}$$

Basically, the EXAFS signal has a sinusoidal behavior, with frequency $2R$ proportional to the inter-atomic distance. The phase of the sine function is perturbed by the phase-shift $\phi(k)$, while the amplitude is modulated by $|f_B(k,\pi)|$.

Backscattering amplitude and phaseshifts

The k dependence of backscattering amplitudes and phaseshifts is different for different atomic species.
The central atom phaseshift δ always decreases monotonously when the wavevector k increases (Fig. 6, right). The modulus of the backscattering amplitude $|f(k,\pi)|$ decreases monotonously for low-Z atomic species; it becomes higher at high k values and progressively more structured when Z increases (Fig. 6, centre). Correspondingly, the backscattering phaseshift exhibits a more structured behaviour when Z increases (Fig. 6, right).
The different behaviour of the backscattering amplitude and phase-shift for different Z values is currently exploited for distinguishing the atomic species of the scattering atom with reasonable approximation.

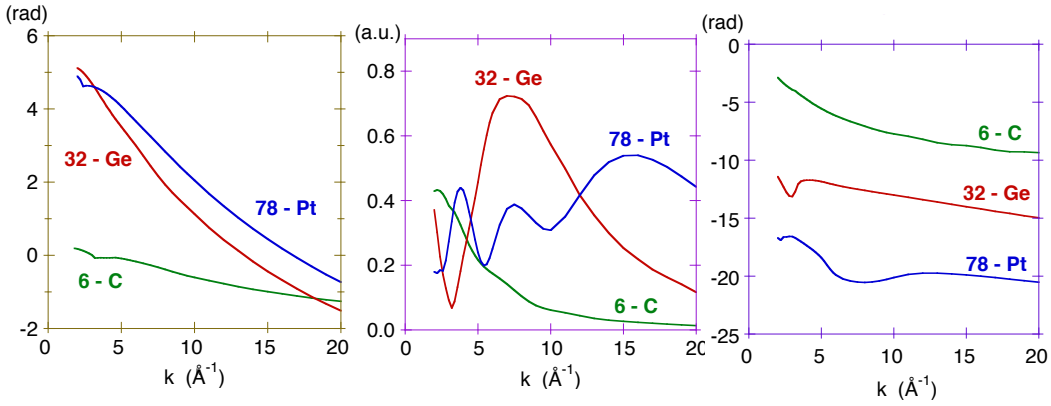

Fig. 6: Central atom phaseshifts (left), backscattering amplitudes (centre) and backscattering phaseshifts (right) calculated for selected atomic species by FEFFIT 6.1 within the plane wave approximation. The total phaseshift $\phi(k)$ of (14) and (15) is the sum of the phaseshifts of the left and right panels.

For realistic spherical waves (say if the plane wave approximation is released), phaseshifts and amplitudes weakly depend also on the interatomic distance: $\phi(k,r)$, $|f(k,\pi,r)|$ [11].

3.2 Many-atomic systems

Let us now consider a system composed of more than two atoms. The generalization of (13) is immediate, so long as multiple scattering events can be neglected: the EXAFS function can be built up as a sum of two-atomic contributions (13), with different interatomic distances R_j from the absorber atom.

Isotropic samples

Very often, EXAFS measurements are performed on isotropic samples, such as polycrystalline powders, amorphous materials, liquids or gases. In the following, we consider only isotropic samples,

for which the polarization term can be averaged, $\langle \hat{\boldsymbol{\eta}} \cdot \hat{\mathbf{R}} \rangle = 1/3$, leading to a simplified treatment which neglects the angular part of the wavefunctions.
For an isotropic sample, the EXAFS function is

$$\chi(k) \;=\; \frac{1}{k} \sum\nolimits_j \frac{1}{R_j^2} \;\mathrm{Im}\; \left\{ f_j(k,\pi)\; e^{2i\delta_1}\; e^{2ikR_j} \right\} , \tag{16}$$

where R_j is the distance of the j-th atom from the absorber atom.

Coordination shells

If atoms can be grouped into coordination shells (Fig. 7), each one containing N_s atoms of the same species at the same distance R_s from the absorber atom, it is convenient to rewrite (13) separating the contributions of the different coordination shell:

$$\chi(k) = \frac{1}{k} \sum_s \frac{N_s}{R_s^2} \;\mathrm{Im}\left\{ f_s(k,\pi)\; e^{2i\delta_1}\; e^{2ikR_s} \right\} . \tag{17}$$

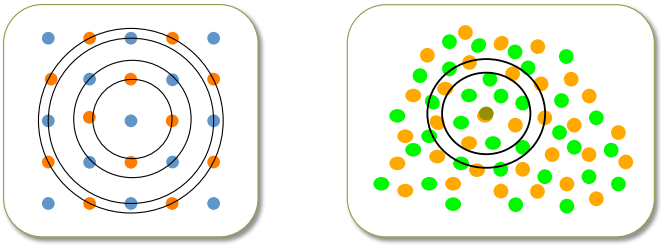

Fig. 7: For crystals (left) the coordination shells of a given atom are in principle perfectly defined at any distance. For non-crystalline systems (right) the coordination shells are quite well defined only at short distances.

The sum in (17) is on the index s, which labels the coordination shells. The parameter N_s is the *coordination number* of shell s.

4 Inelastic effects

As it was shown in Part 2 (Photoelectric absorption of X-rays), the total absorption cross section is the sum of two terms,

$$\sigma_a(\omega) \;=\; \sigma_{\mathrm{el}}(\omega) \;+\; \sigma_{\mathrm{inel}}(\omega) . \tag{18}$$

The treatment that leads to (17) is based on elastic (fully relaxed) transitions and corresponds to the first term on the right of (18). Let us now study how inelastic phenomena affect the EXAFS signal. Two types of inelastic effects have to be distinguished:

a) intrinsic effects, which are many-body interactions within the absorber atom and correspond to σ_{inel} in (18);
b) extrinsic effects, which are many-body interactions of the photoelectron with electrons not belonging to the emitting atom.

4.1 Intrinsic inelastic effects

In the inelastic excitation channels of the X-ray absorption process, the relaxation of the $N-1$ passive electrons is accompanied by their excitation (shake-up and shake-off processes). The X-ray photon energy is distributed over all the excited electrons, and the photoelectron has a distribution of possible energies, so that the corresponding EXAFS signals sum up incoherently and give rise to a damping of the experimentally observed oscillations.

The net effect is a reduction of the coherent EXAFS signal with respect to that calculated for purely elastic excitations in (17). One can show that the fraction of the total cross section (18) that corresponds to the elastic channel $\sigma_{\rm el}$ is measured by the superposition integral of the passive electrons wavefunctions

$$S_0^2 \;=\; \left| \langle\, \Psi_{f,r}^{N-1} | \Psi_i^{N-1} \,\rangle \right|^2 . \tag{19}$$

In order to reproduce an experimental signal, the EXAFS function (17), based on the elastic cross section, has to multiplied by the factor S_0^2, which typically amounts to $0.7 \div 0.9$.

4.2 Extrinsic inelastic effects: mean free path

Extrinsic inelastic effects are losses of the energy of the photoelectron during its propagation, due to excitations (core-hole and plasmons) and inelastic scattering by other single electrons.
From a phenomenological point of view, the extrinsic inelastic losses are measured by a k-dependent mean free path $\lambda(k)$ (don't confuse λ with the photo-electron wavelength).
Two distinct phenomena contribute to the total mean free path λ:

a) the core-hole lifetime τ_h, which depends on the atomic number Z (the higher Z, the shorter τ_h) and establishes the distance $\lambda_h = v\tau_h$ the photo-electron can travel before the de-excitation of the absorber atom;
b) the energy-dependent photo-electron mean-free path λ_e, determined by the inelastic interactions with single electrons and collective excitations (plasmons).

The smaller of the two contributions determines the actual value of λ, according to:

$$\frac{1}{\lambda} \;=\; \frac{1}{\lambda_h} \;+\; \frac{1}{\lambda_e}. \tag{20}$$

At low energies, in the XANES region, the mean free path is determined by λ_h, while in the EXAFS region the contribution of λ_e is predominant (Fig. 8).
The mean free path measures the average distance an excited electron can travel before losing coherence with its initial state.

The extrinsic inelastic effects are generally taken into account in the EXAFS formula by a phenomenological factor $\exp[-2R_j\lambda(k)]$, where $\lambda \simeq 5-15$ Å. The mean free path factor progressively reduces the amplitude of EXAFS oscillations when R_j increases, contributing to making EXAFS insensitive to long range order.

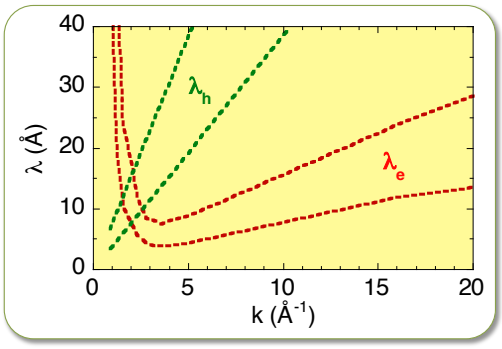

Fig. 8: Mean free path as a function of the wavevector k. The values λ_e measured for different elements are included between the two continuos lines. The dashed lines include the λ_h values for the K edges of atoms with Z between 30 and 50.

4.3 EXAFS formula including inelastic effects

To summarize, the EXAFS equation taking into account inelastic effects is:

$$\chi(k) \;=\; \frac{S_0^2}{k} \sum\nolimits_j \frac{e^{-2R_j/\lambda}}{R_j^2} \;\mathrm{Im}\; \left\{ f_j(k,\pi)\; e^{2i\delta_1}\; e^{2ikR_j} \right\} . \tag{21}$$

If atoms can be grouped into coordination shells, one can rewrite Eq. (21) separating the contributions of different coordination shell, as in (17):

$$\chi(k) = \frac{S_o^2}{k} \sum_s N_s \;\mathrm{Im} \left\{ f_s(k,\pi)\; e^{2i\delta_1}\; \frac{e^{-2R_s/\lambda}}{R_s^2}\; e^{2ikR_s} \right\} . \tag{22}$$

5 Multiple scattering

Up to now, we have considered only single scattering (SS) paths of the photo-electron, consisting in two "legs", the first one from the the emitting atom A to the scattering atoms B, the second one from the scattering atom B back to the emitting atom A (two examples are shown in the rigth panel of Fig. 9).

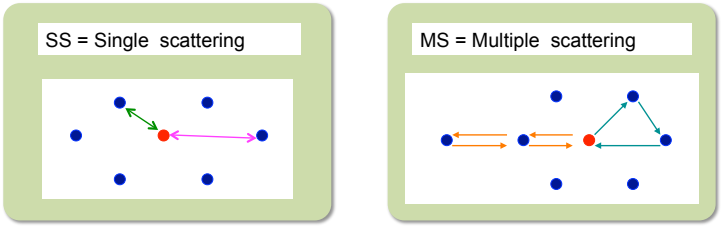

Fig. 9: Left: possible single scattering paths originating from and terminating at a given central atom (red). Right: possible multiple scattering paths originating from and terminating at a given central atom (red).

Actually, multiple scattering (MS) paths are possible too, where the photoelectron is scattered by two or more atoms before coming back to the emitting atom A. Two significant examples are shown in the right panel of Fig. 9): *a)* a triangular path $A \to B \to C \to A$ and *b)* a collinear path $A \to B \to C \to B \to A$, where the photoelectron is forward scattered by atom B.
Multiple scattering events are very important in the XANES region, due to the relatively low energy of the photoelectron. They are generally quite weak in the EXAFS region, but not at all negligible; particularly strong is the contribution of collinear MS paths, due to the high amplitude for scattering at 180° (forward scattering).

To take into account MS effects, the absorption coefficient is conveniently written as

$$\mu(k) \;=\; \mu_0(k)\,[1 + \chi_2(k) + \chi_3(k) + \chi_4(k) + \cdots] , \tag{23}$$

where the terms χ_p of the sum are distinguished by the number p of legs of the scattering paths. The term $\chi_2(k) \equiv \chi(k)$ corresponds to the single scattering contributions up to now considered. In the EXAFS region, the series (23) is fast convergent. The convergence becomes progressively slower when the wavevector k decreases, say approaching the XANES region.
It has been demontrated [11] that the contribution of MS paths to the EXAFS signal can be expressed, similar to the SS contribution, as the product of an amplitude factor and an oscillating factor; for a given path p,

$$\chi_p(k) \;=\; A_p(k, \{\mathbf{r}\}_p)\, \sin\left[kR_p + \phi_p(k, \{\mathbf{r}\}_p)\right] , \tag{24}$$

where $\{\mathbf{r}\}_p$ represents the set of all vector distances inside the path, R_p is the total path length, and A_p and ϕ_p are effective amplitude and phaseshift functions which depend on the potential acting on the photo-electron.

6 Disorder effects on EXAFS

Equation (22) refers to the unphysical situation of a system where the atoms are frozen at their equilibrium positions.

Thermal disorder

In real systems, atoms are affected by thermal vibrations, whose amplitude increases with temperature but, for quantum reasons, is not negligible even near zero kelvin. The instantaneous positions of atoms are spread around the equilibrium positions according to statistical distributions (thermal ellipsoids, left panel of Fig. 10).
The period of atomic vibrations ($\simeq 10^{-12}$ s) is much larger than the photo-electron time of flight ($10^{-16} \div 10^{-15}$ s). A single photo-electron samples an instantaneous distance between emitting and backscattering atom (Fig. 10, left). An EXAFS spectrum, resulting from the contributions of a large number of photo-electrons, samples a *distribution* of instantaneous interatomic distances r for each coordination shell (Fig. 10, righ1).

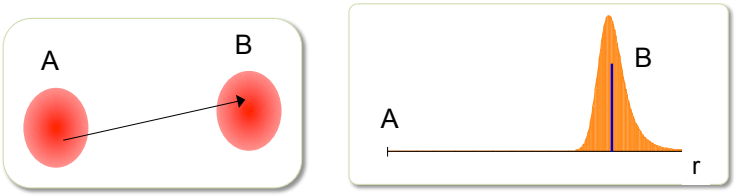

Fig. 10: Left: a single photoelectron samples an instantaneous relative distance r between the thermal ellipsoids of the emitting and the backscattering atoms. Right: and EXAFS spectrum samples a one-dimensional distribution of instantamneous distances.

Structural disorder

The distribution of interatomic distances can be further enlarged and modified by the presence of structural disorder. Some examples of structural disorder are schematically depicted in Fig. 11.

a) Distorted coordination shells in crystals are characterised by the presence of two or more slightly different interatomic distance, which cannot be experimentally discriminated as different coordination shells.
b) In some crystalline systems, the absorber atom can be found in two or more structurally different sites, which again cannot be discriminated as different coordination shells (*sites disorder*).
c) In non-crystalline systems, the nearest-neighbour coordination is very similar to that in the corresponding crystals, the inter-atomic pair distances are however not exactly equal.
d) In nano-crystals, the distances between nearest-neighbour atoms are different according to whether the atomic pair is near the surface or at the centre of the cluster; one thus expects a static distribution of distances, to be convoluted with the distribution due to thermal motion.

A peculiar kind of disorder is **compositional disorder**, consisting in the presence of atoms of different species in the same coordination shell.

6.1 EXAFS formula for disordered systems

Let us consider here only coordination shells containing *one atomic species* (say without compositional disorder).
Due to disorder, the contribution to the EXAFS function of a given coordination shell (or more generally of a given scattering paths) can be expressed in terms a configurational average of the

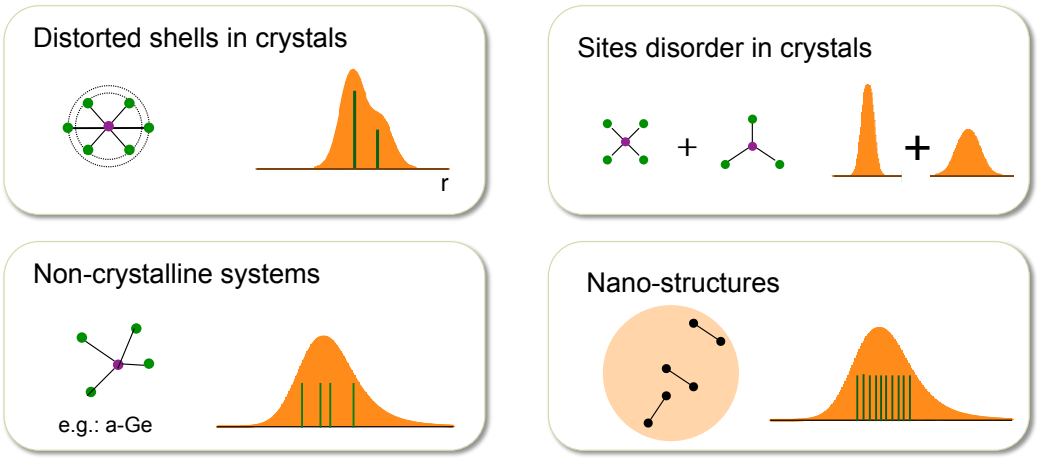

Fig. 11: Some examples of structural disorder that can contribute to enlarge the distribution of distances due to thermal disorder.

distance-dependent factors [12]:

$$\chi_s(k) = \frac{S_o^2}{k}\, N_s\, \mathrm{Im}\left\{ f_s(k,\pi)\, e^{2i\delta_1} \left\langle \frac{e^{-2r/\lambda}}{r^2}\, e^{2ikr} \right\rangle dr \right\}. \tag{25}$$

In the case of purely thermal disorder, with no structural contributions, the brackets $\langle\ \rangle$ in Eq. (25) indicate a canonical average.

Equivalentlyly, the distance between absorber and back-scatterer atoms of a given coordination shell, instead of having a single value R_s, like in (22), varies according to a probability distribution $\rho(r)$, normalized to unity, and the EXAFS signal is generated from an average over this distribution. The EXAFS equation for one coordination shell becomes [13]

$$\chi_s(k) = \frac{S_o^2}{k}\, N_s\, \mathrm{Im}\left\{ f_s(k,\pi)\, e^{2i\delta_1} \int_0^\infty \rho(r)\, \frac{e^{-2r/\lambda}}{r^2}\, e^{2ikr}\, dr \right\}. \tag{26}$$

Real and effective distributions

The distribution $\rho(r)$ in Eq. (26) is commonly referred to as *real distribution* and corresponds to the partial radial distribution function (RDF) around the absorbing atomic species.
It is convenient to group all r-dependent factors into an *effective distribution*

$$P(r,\lambda) = \rho(r)\, \frac{e^{-2r/\lambda}}{r^2}, \tag{27}$$

so that the EXAFS equation can be rewritten as

$$\chi_s(k) = \frac{S_o^2}{k}\, N_s\, \mathrm{Im}\left\{ f_s(k,\pi)\, e^{2i\delta_1} \int_0^\infty P(r,\lambda)\, e^{2ikr}\, dr \right\}. \tag{28}$$

The difference between real and effective distributions is physically due to the progressive attenuation of the photoelectron spherical wave with distance: the low-r part of the real distribution has a higher weight than the high-r part (Fig. 12).

The inversion problem

The integral in Eq. (28) is the Fourier transform of the effective distribution $P(r,\lambda)$, or, in the probability language, its *characteristic function*. The conjugate variable is $2k$. The characteristic function is a complex function of a complex variable; its full knowledge is equivalent to the knowledge of the distribution $P(r,\lambda)$.

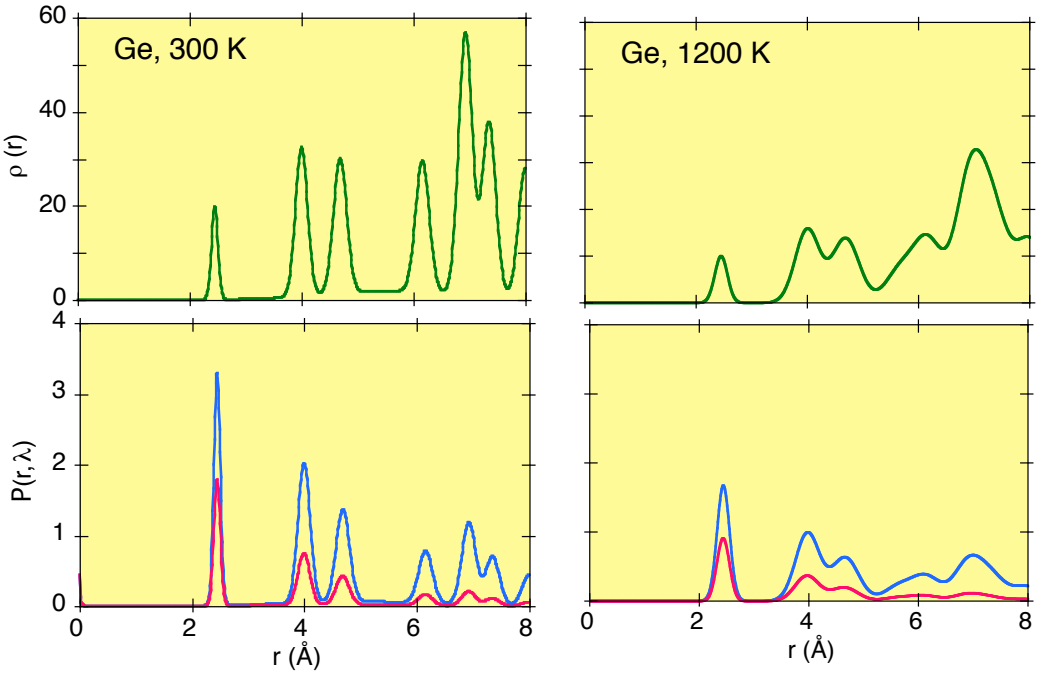

Fig. 12: Top panels: simulation of the real distribution $\rho(r)$ for germanium at 300 K (left) and at 1200 K (right). Bottom panels: corresponding distributions $\rho(r)/r^2$ (blue lines) and $P(r,\lambda) = \rho(r)\exp(-2r/\lambda)/r^2$, evidencing the effects of the spherical wave attenuation and of the mean free path.

The fundamental problem of EXAFS analysis is to recover the effective distribution $P(r,\lambda)$, and hence the real distribution $\rho(r)$, from the experimental spectrum $\chi(k)$.
No exact solution can be given to this problem, because an experimental spectrum never corresponds to the full characteristic function, as expressed by Eq. (28), but has a finite extension, included between the values $k_{\min}$ and $k_{\max}$. In particular, for $k_{\min} \leq 2 \div 3$ Å^{-1} the EXAFS signal generally cannot be utilized, due to: *a)* difficulty in determining the atomic absorption coefficient μ_0 in the vicinity of the edge, *b)* effects of the core-hole lifetime on the low-energy electrons, *c)* influence of multiple scattering processes.

The problem of recovering $\rho(r)$ from $\chi(k)$ is generally solved by hypothesising physically sound structural models and optimising the parameters of their distributions $\rho(r)$ by best fit of eq. (26) to the experimental EXAFS spectrum [14].

For weak disorder, the distributions of distances (both real and effective) can be parameterised in terms of a few statistical parameters, called cumulants, which are linear combinations of the more familiar moments. Correspondingly, the EXAFS signal can be expressed in terms of a few leading cumulants, as is shown below.

7 Parametrization of EXAFS formula

For many applications, the extent of disorder is sufficiently small to allow the expression of the EXAFS formula in terms of a few standard parameters. In such cases, the EXAFS function for a given coordination shell (or for a given scattering path) can be expressed as

$$\chi_s(k) = \frac{S_o^2}{k}\, N_s\, |f_s(k,\pi)|\, \frac{e^{-2C_1/\lambda}}{C_1^2}\, e^{-2k^2C_2+2k^4C_4/3\cdots}\, \sin\left[2kC_1 - \frac{4k^3C_3}{3} \ldots + \phi(k)\right], \qquad (29)$$

where the parameters C_i are the cumulants of the *effective* distribution $P(r,\lambda)$ [15, 16].

According to the probability theory, the cumulants characterise the position, width and shape of a distribution; in particular, C_1 is the mean value, C_2 is the variance and C_3 is a measure of the asymmetry of the distribution.
It is worth noting that even and odd cumulants determine the amplitude and the phase of the EXAFS signal, respectively.

Parameters of the real distribution

Actually, one is interested in the cumulants C_i^* of the *real* distribution $\rho(r)$. The first cumulant C_1^* of the real distribution $\rho(r)$ is significantly larger than the first cumulant C_1 of the effective distribution, as a consequence of the spherical nature of the photo-electron wave and its limited mean free path:

$$C_1^* \simeq C_1 + \frac{2C_2}{C_1}\left(1 + \frac{C_1}{\lambda}\right) . \tag{30}$$

The difference, of the order of some 10^{-3} Å, is automatically taken into account by most data analysis packages. The difference between higher-order cumulants of the two distributions is generally negligible.

The lowest-order cumulants of the real distribution have simple interpretations:

1. The first cumulant $C_1^* = \langle r \rangle$ is the mean value of the distribution, say the average inter-atomic distance.
2. The second cumulant $C_2^* = \sigma^2 = \langle (r - \langle r \rangle)^2 \rangle$ is the variance of the distribution or mean square relative displacement (MSRD); the exponential $\exp(-2k^2\sigma^2)$ of (29) is referred to as EXAFS Debye-Waller factor.
3. The third cumulant $C_3^* = \mu_3 = \langle (r - \langle r \rangle)^3 \rangle$ is the mean cubic relative displacement and measures the distribution asymmetry.
4. The fourth cumulant C_4^* measures the flatness of the distribution, say the symmetric deviation with respect to a gaussian shape.

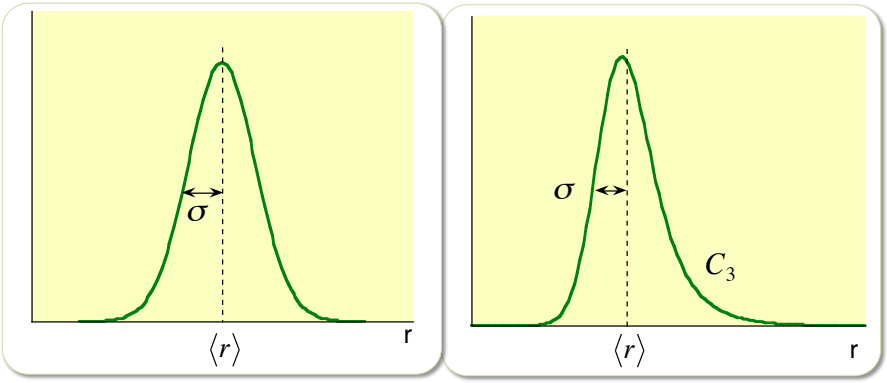

Fig. 13: Symmetric distribution (left) and asymmetric distribution (right).

In some cases, the cumulant expansion can be truncated at the second order term, and eq. (29) reduces to the so called standard EXAFS formula

$$\chi_s(k) = \frac{S_o^2}{k} N_s |f_s(k,\pi)| \frac{e^{-2C_1/\lambda}}{C_1^2} e^{-2k^2C_2} \sin\left[2kC_1 + \phi(k)\right] , \tag{31}$$

which amounts to consider a gaussian effective distribution $P(r,\lambda)$, which corresponds with good approximation to a gaussian real distribution $\rho(r)$ (Fig. 13, left):

$$\rho(r) = (1/\sigma\sqrt{2\pi}) \exp\left[-(r - \langle r \rangle)^2/2\sigma^2\right] , \tag{32}$$

where $C_1^* = \langle r \rangle$ is the average distance and $C_2^* = \sigma^2 = \langle (r - \langle r \rangle)^2 \rangle$ is the variance. The gaussian approximation, generally reliable for the second and outer coordination shells, is unfit for the first coordination shell, where the asymmetry of the pair interaction potential is more influent.

For the first coordination shell it is higly recommended to add the third cumulant $C_3^* = \langle (r - \langle r \rangle)^3 \rangle$ (mean cubic relative displacement) to account for the distribution asymmetry (Fig. 13, right):

$$\chi_s(k) = \frac{S_o^2}{k} \; N_s \; |f_s(k,\pi)| \; \frac{e^{-2C_1/\lambda}}{C_1^2} \; e^{-2k^2 C_2} \; \sin\left[2kC_1 - \frac{4k^3 C_3}{3} + \phi(k)\right] . \tag{33}$$

8 Summary

Using (29), or the more approximate expressions (32) or (33)), one can get original information on the local structure from the analysis of EXAFS, provided some "physical" quantities are known: phaseshifts, backscattering amplitude, inelastic terms.

8.1 Structural parameters

An EXAFS experiment samples a one-dimensional distribution of interatomic distances, which contains the contributions of all single and multiple scattering paths originating and terminating at the absorbing atom, within the reduced range determined by the spherical nature of the photoelectron wave and by its mean free path.

The following structural parameters can in principle be obtained for each coordination shell of the absorbing atom, considering only single scattering contributions to the EXAFS signal.

a) *Coordination number.* The amplitude of the EXAFS signal is directly proportional to the number N_s of atoms within the shell.

b) *Average inter-atomic distance.* The frequency of the EXAFS signal depends on the first cumulant C_1 of the effective distribution, which is connected by (30) to the average interatomic distance $\langle r \rangle$.
The argument of the sine function in (29) depends also on the third cumulant (and possibly on higher order odd cumulants); neglecting the third cumulant in the analysis can severely affect the accuracy of the value $\langle r \rangle$ for the first coordination shell.

c) *Debye-Waller factor.* The second cumulant $C_2 = \sigma^2$ (Debye-Waller exponent) corresponds to the *mean square relative displacement* (MSRD) of absorber and back-scatterer atoms.
The Debye-Waller factor $\exp[-2k^2\sigma^2]$ causes a damping of the EXAFS signal. The value of σ^2 increases with increasing temperature. Its temperature dependence gives original information on the local vibrational dynamics.

d) *Third cumulant.* The third cumulant measures the asymmetry of the distribution of distances. It is significant for the first coordination shell, but seems to be negligible for the outer coordination shells.

8.2 Phase-shifts, back-scattering amplitudes and inelastic terms

Two different procedures can be used to insert into Eq. (29) the "physical quantities" $|f(k,\pi)|$, ϕ, S_0^2 and λ for each coordination shell.

1. The "physical quantities" are experimentally obtained from the EXAFS of a reference sample of known structure. The local structure of the reference sample should be as much as possible similar to that of the unknown sample, in order to guarantee the *amplitude and phase-shift transferability.*
2. The "physical quantities" are calculated ab-initio [11] by a number of easily available software packages [17, 18, 19], with a degree of accuracy sufficient for most applications.

References

[1] NIST, "X-ray mass attenuation coefficients," 2004. http://www.nist.gov/pml/data/xraycoef/.

[2] C. T. Chantler, C. Q. Tran, Z. Barnea, D. Paterson, D. J. Cookson, and D. X. Balaic, "Measurement of the x-ray mass attenuation coefcient of copper using 8.85 20 kev synchrotron radiation," *Phys. Rev. A*, vol. 64, p. 062506, 2001.

[3] J. Padežnik Gomilšek, A. Kodre, I. Arčon, and G. Bratina, "X-ray absorption of cadmium in the l-edge region," *Phys. Rev. A*, vol. 84, p. 052508, 2011.

[4] C. T. Chantler, M. T. Islam, N. A. Rae, C. Q. Tran, J. L. Glover, and Z. Barnea, "New consistency tests for high-accuracy measurements of x-ray mass attenuation coefficients by the x-ray extended-range technique.," *Acta Cryst. A*, vol. 68, pp. 188–195, 2012.

[5] J. Als-Nielsen and D. McMorrow, *Elements of Modern X-ray Physics*. Chichester, UK: John Wiley & Sons, 2011.

[6] P. A. Lee, P. H. Citrin, P. Eisenberger, and B. M. Kincaid, "Extended x-ray absorption fine structure, its strengths and limitations," *Rev. Mod. Phys.*, vol. 53, pp. 769–806, 1981.

[7] T. M. Hayes and J. B. Boyce, "Extended x-ray-absorption fine structure spectroscopy," *Solid State Physics*, vol. 37, pp. 173–350, 1982.

[8] E. A. Stern, "Theory of extended x-ray fine structure," *Phys. Rev. B*, vol. 10, pp. 3027–3037, 1974.

[9] I. B. Borovskii, R. V. Vedrinskii, V. L. Kraizman, and V. P. Sachenko, "Exafs spectroscopy: a new method for structural investigation," *Sov. Phys. Usp.*, vol. 29, pp. 539–569, 1986.

[10] G. J. Joachain, *Quantum Collision Theory*. North Holland, 1975.

[11] J. J. Rehr and R. C. Albers, "Theoretical approaches to x-ray absorption fine structure," *Rev. Mod. Phys.*, vol. 72, pp. 621–654, 2000.

[12] J. Freund, R. Ingalls, and E. D. Crozier, "Extended x-ray absorption fine structure study of copper under high pressure," *Phys. Rev. B*, vol. 39, pp. 12537–12547, 1989.

[13] E. A. Stern, D. E. Sayers, and F. W. Lytle, "Extended x-ray-absorption fine-structure technique. iii. determination of physical parameters," *Phys. Rev. B*, vol. 11, pp. 4836–4846, 1975.

[14] A. Filipponi, "Exafs for liquids," *J. Phys.: Condens. Matter*, vol. 13, pp. R1–R38, 2001.

[15] G. Bunker, "Application of the ratio method of exafs analysis to disordered systems," *Nucl. Instrum. Methods Phys. Res.*, vol. 207, pp. 437–444, 1983.

[16] P. Fornasini, F. Monti, and A. Sanson, "On the cumulant analysis of exafs in crystalline solids," *J. Synchrotron Radiat.*, vol. 8, pp. 1214–1220, 2001.

[17] XAFS software, "Catalog home page." http://www.esrf.eu/Instrumentation/software/data-analysis/Links/xafs.

[18] GNXAS, "Home page." http://gnxas.unicam.it/.

[19] FEFF, "Project home page." http://feffproject.org.